Applied Catalysis B: Environmental 168-169 (2015) 1–8

Contents lists available at ScienceDirect

Applied Catalysis B: Environmental

journal homepage: www.elsevier.com/locate/apcatb

High-efficiency conversion of CO_2 to fuel over ZnO/g-C_3N_4 photocatalyst

Yiming He [a,b], Yan Wang [a], Lihong Zhang [b], Botao Teng [a,c], Maohong Fan [a,d,*]

[a] School of Energy Resources, University of Wyoming, Laramie, WY 82071, USA
[b] Department of Materials Physics, Zhejiang Normal University, Jinhua 321004, China
[c] College of Chemistry and Life Sciences, Zhejiang Normal University, Jinhua 321004, China
[d] School of Civil and Environmental Engineering, Georgia Institute of Technology, Atlanta, GA 30332, USA

ARTICLE INFO

Article history:
Received 3 July 2014
Received in revised form 3 November 2014
Accepted 12 December 2014
Available online 17 December 2014

Keywords:
CO_2
Photocatalysis
ZnO/g-C_3N_4
Fuel

ABSTRACT

The objective of this research was to prepare, characterize and evaluate the conversion efficiency of CO_2 to fuel on a ZnO/g-C_3N_4 composite photocatalyst under simulated sunlight irradiation. The photocatalyst was synthesized by a simple impregnation method and was characterized by various techniques, including Brunauer–Emmett–Teller method (BET), X-ray diffraction (XRD), Fourier transform infrared spectroscopy (FT-IR), scanning electron microscopy (SEM), transmission electron microscopy (TEM), X-ray photoelectron spectroscopy (XPS), UV–vis diffuse reflectance spectroscopy (DRS), and photoluminescence spectroscopy (PL). The characterizations indicate that ZnO and g-C_3N_4 were uniformly combined. The deposition of ZnO on g-C_3N_4 showed nearly no effect on its light-absorption performance. However, the interactions between the two components promoted the formation of a hetero-junction structure in the composite, inhibited the recombination of electron–hole pairs and, finally, enhanced the photocatalytic performance of ZnO/g-C_3N_4. The optimal ZnO/g-C_3N_4 photocatalyst showed a CO_2 conversion rate of 45.6 μmol h^{-1} g_{cat}^{-1}, which was 4.9 and 6.4 times higher than those of g-C_3N_4 and P25, respectively. This work represents an important step toward artificial photocatalytic CO_2 conversion to fuel using cost-efficient materials.

1. Introduction

Two urgent challenges currently confront humanity. The first is to seek a clean and sustainable alternative energy source, due to the decreasing availability of fossil fuels; the other is the rapid increase in CO_2 emissions believed to be the primary cause of global warming. Several approaches have been suggested to address these challenges. Among these are CO_2 capture and storage, as well as solar-photovoltaic cells and solar fuels, including hydrogen generation from photocatalytic water splitting and carbon-based fuels from photocatalytic CO_2 reduction. Of these, converting CO_2 into useful chemicals and clean fuels (e.g., CO, CH_4 or CH_3OH) is a highly promising approach that might simultaneously address both challenges. Since Halmann and Inoue et al. first reported the photocatalytic reduction of CO_2 in the late 1970s [1,2], scientists have made various attempts in the photocatalytic conversion of CO_2 [3–9]. Although TiO_2 is the most popular photocatalyst due to its robust reactivity, commercial availability and chemical stability, it can absorb only ultraviolet (UV) light, which occupies no more than 4% of the solar spectrum, thus significantly limiting its application. Therefore, the development of an efficient photocatalyst with high activity under sunlight is needed.

Due to its moderate band gap (E_g = 2.7 eV) and high stability, graphitic carbon nitride (g-C_3N_4) has recently attracted significant attention as a novel, metal-free semiconductor. Wang et al. [10] first reported that g-C_3N_4 has high photocatalytic performance for hydrogen or oxygen production from water splitting under visible-light irradiation. The application of g-C_3N_4 in water purification and CO_2 photoreduction has also been reported [11,12]. And since it can be easily prepared via heating melamine or urea, g-C_3N_4 is cheaper than TiO_2. In addition, g-C_3N_4 has a much more negative conduction band (E_{cb} = −1.20 V) [10] than TiO_2 (E_{cb} = −0.29 V) [13], which means that its photogenerated electrons have stronger reducibility, allowing it to reduce CO_2 to CH_3OH $E_{CO_2}/CH_3OH = -0.32V$ or other hydrocarbon fuels [6] that cannot be generated over a TiO_2 photocatalyst. However, despite its potential for CO_2 photoreduction, the photocatalytic activity of g-C_3N_4 in CO_2 reduction is

* Corresponding author at: School of Energy Resources, University of Wyoming, Laramie, WY 82071, USA. Tel.: +1 307 766 5633; fax: +1 307 766 6667.
E-mail address: mfan@uwyo.edu (M. Fan).

http://dx.doi.org/10.1016/j.apcatb.2014.12.017
0926-3373/

still low, necessitating the modification of g-C_3N_4 to improve its photocatalytic efficiency. The approach of coupling g-C_3N_4 with another semiconductor to construct a hetero-junction composite has been proven effective [14–17]. For example, Cao et al. reported that the doping of In_2O_3 on g-C_3N_4 could increase CH_4 yield by a factor of three [16]. Yuan et al. used red phosphor (P) to modify g-C_3N_4, yielding twice the CH_4 from the hybrid than from pure P and nearly three times more than pure g-C_3N_4 [17]. Zou et al. synthesized g-C_3N_4/N-TiO_2 composite by a simple pyrolysis process of urea and $Ti(OH)_4$. The prepared composite was proved to be an effective photocatalyst for the selective reduction of CO_2 to CO [18]. However, the photocatalytic activity of the reported photocatalysts was still too low to be applied practically, and only a few investigations focused on the photoreduction of CO_2 over g-C_3N_4-based photocatalysts. One possible reason for this is that the photogenerated electrons typically accumulate on the coupled semiconductors of the g-C_3N_4-based composites, which would significantly decrease the reducibility of electrons, especially when the coupled semiconductors have a low conduction band, such as with WO_3, $BiVO_4$, and Ag_3VO_4. And although these composite photocatalysts are effective in dye degradation [19–21], they are not suitable for photocatalytic H_2 generation or CO_2 conversion.

Unlike the aforementioned semiconductors, however, ZnO has a conduction band with a negative potential (E_{CB} = −0.44 eV) and can photocatalytically reduce CO_2 to CO or CH_4 [2,22]. In addition, ZnO is an amphoteric oxide and has moderate ability to absorb CO_2, which is beneficial for photoreaction. Hence, ZnO coupled with g-C_3N_4 might be an effective photocatalyst for CO_2 reduction. Indeed, a ZnO/g-C_3N_4 composite has been previously reported, as both Wang et al. and Liu et al. synthesized a ZnO photocatalyst hybridized with g-C_3N_4 using a milling-heat treatment method [23,24]. In addition, Sun reported a ZnO/g-C_3N_4 composite photocatalyst synthesized by directly heating melamine and zinc acetate [25]. All of the obtained ZnO/g-C_3N_4 composites were applied in photocatalytic dye degradation and exhibited superior activity compared to g-C_3N_4 or ZnO alone. However, to the best of our knowledge, no research on photocatalytic CO_2 conversion on a ZnO/g-C_3N_4 composite has been reported.

In this paper, a ZnO/g-C_3N_4 composite photocatalyst was synthesized by an impregnation method, and its catalytic ability was investigated through photocatalytic CO_2 conversion. Porous g-C_3N_4 with a high surface area was used as the support. The loading of ZnO markedly increased the activity of g-C_3N_4 on photocatalytic CO_2 conversion. With the help of a thorough investigation of the composite's structure, surface area and optical properties, the origin of the higher photoactivity of the ZnO/g-C_3N_4 composite was documented.

2. Experimental

2.1. Preparation of the ZnO/g-C_3N_4 photocatalyst

Zinc acetate ($Zn(OOCCH_3)_2{\cdot}2H_2O$, >98%) and urea ($NH_2CONH_2$, >99%) were purchased from the Alfa-Aesar company. ZnO was prepared by heating zinc acetate at 300 °C for 2 h. Pure g-C_3N_4 was synthesized by heating urea at 550 °C for 4 h. A ZnO/g-C_3N_4 composite was prepared by an impregnation method. Typically, different amounts of zinc acetate were dissolved in 2 mL deionized water, after which, 0.15 g of g-C_3N_4 was added. The resulting mixture was allowed to set at room temperature for 4 h. The water in the solution was then evaporated at 60 °C. After drying at 80 °C for 12 h, the sample was calcined at 300 °C for 2 h to obtain the final ZnO/g-C_3N_4 photocatalysts. Through this method, samples with different ZnO to g-C_3N_4 weight ratios (i.e., 2 wt.%, 4 wt.%, 6 wt.% and 8 wt.% ZnO/g-C_3N_4) were obtained and labeled as 2ZC, 4ZC, 6ZC and 8ZC, respectively. For comparison, a physical mixture of ZnO and g-C_3N_4 with the same ZnO concentration as the 6 wt.% ZnO/g-C_3N_4 composite was also prepared by simple grinding in an agate mortar for 10 min.

2.2. Characterizations of photocatalysts

The BET surface area of the samples was measured by a Quantachrome Autosorb IQ automated gas sorption analyzer with an outgas temperature of 150 °C for 3 h and a N_2 adsorption–desorption isotherm. The XRD data were collected using a Rigaku Smart Lab automated powder diffraction system in the range of 10–70°. The FT-IR spectra of the catalysts were recorded on a Nicolet iS50 FT-IR spectrometer with a resolution of 4 cm^{-1}. The XPS measurements were performed using a Physical Electronics ESCA 5800 spectrometer. Adventitious carbon was added to determine the induced offset of the binding energy (BE) of the C1s peak (284.6 eV) due to surface charging effects. The SEM images were taken by a FEI Quanta 450 field emission scanning electron microscope. The TEM images were obtained with a JEM-2010F transmission electron microscope at an accelerating voltage of 200 kV. The DRS spectra of catalysts were performed on a Cary 4000 UV–vis spectrophotometer (Varian) using MgO as reference. The PL spectra were collected on an Edinburgh FLS-920 spectrometer, using a Xe lamp (excitation at 365 nm) as light source.

Electrochemical measurements were performed by a CHI 660B electrochemical workstation with a standard three-electrode cell at room temperature. The prepared sample, an Ag/AgCl electrode (saturated KCl), and a Pt wire were used as the working electrode, the reference electrode, and the counter electrode, respectively. The preparation of working electrodes was based upon the reported literature [26,27]. Electrochemical impedance spectroscopy (EIS) was performed by applying an AC voltage of 10 mV amplitude in the frequency range of 10^5 Hz to 10^{-2} Hz with the initial potential (0 V) in 0.01 M Na_2SO_4. For photocurrent (PC) measurement, a 350 W Xe arc lamp served as light source, and a Na_2SO_4 (0.5 M) aqueous solution was used as the electrolyte.

2.3. Photocatalytic experiments

The photocatalytic CO_2 reduction experiments were carried out in a stainless steel reactor (volume, ~132 mL) with a quartz window on the top of the reactor (see Fig. S1). A 500 W Xe lamp was used as a light source, and the light intensity at the position of the catalyst

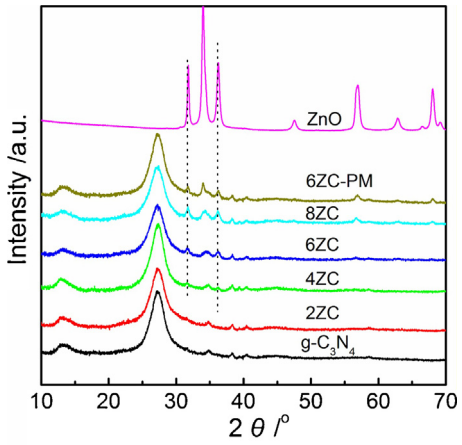

Fig. 1. XRD patterns of ZnO, g-C_3N_4, 6ZC-PM and ZnO/g-C_3N_4 composites with different ZnO concentration.

was 175 mW/cm^2. For the reaction under visible light, a UV cutoff filter was used to remove the UV light ($\lambda < 420$ nm), decreasing light intensity to 105 mW/cm^2. In the photocatalytic CO_2 reduction system, 10 mg of solid catalyst was placed on a Teflon catalyst holder in the upper region of the reactor, and 4 mL deionized water was pre-injected into the bottom of the reactor. Prior to light irradiation, the above system was thoroughly purged by CO_2 to remove air from inside the reactor. During reaction, the CO_2 pressure was regulated at 0.4 MPa and the photoreaction temperature was kept at 80 °C. After light irradiation for 4 h, the gas product was analyzed by an SRI 8610C gas chromatograph with two FID detectors and one TCD detector. The equipped columns were a 6′ MS-13X, a 6′ HAYESEP-D and a 60 M MXT-1, respectively.

3. Results and discussion

3.1. Characteristics of ZnO/g-C_3N_4 composites

The structure of ZnO/g-C_3N_4 composites was characterized by FT-IR and XRD. Pure g-C_3N_4 has a much stronger IR response than ZnO, and the addition of ZnO shows no effect on the IR spectrum of g-C_3N_4 (see Fig. S2). Unlike the FT-IR spectra, the phase change can be clearly observed in the XRD patterns (Fig. 1). As seen in Fig. 1, pure g-C_3N_4 shows two pronounced diffraction peaks at 27.4° and 13.1°, corresponding to (1 0 0) and (0 0 2) crystal planes of the layered g-C_3N_4, respectively [8]. The XRD patterns of ZnO exhibit seven distinct diffraction peaks at 31.8°, 34.0°, 36.3°, 47.5°, 56.9°, 62.9°, and 68.0°, indicating its hexagonal structure (JCPDS No. 36-1451).

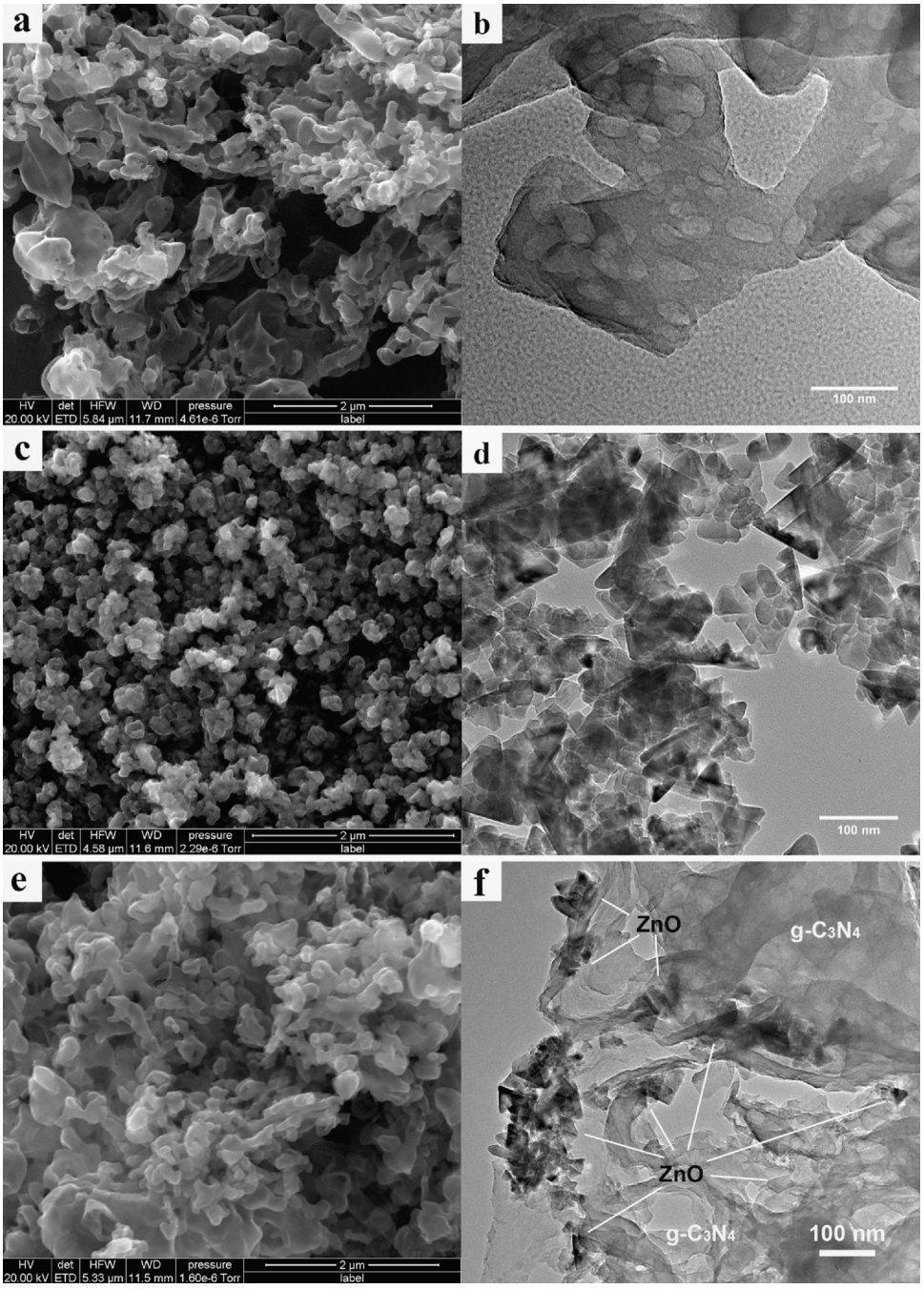

Fig. 2. SEM and TEM images of g-C_3N_4 (a,b), ZnO (c,d), and 6ZC composite (e,f).

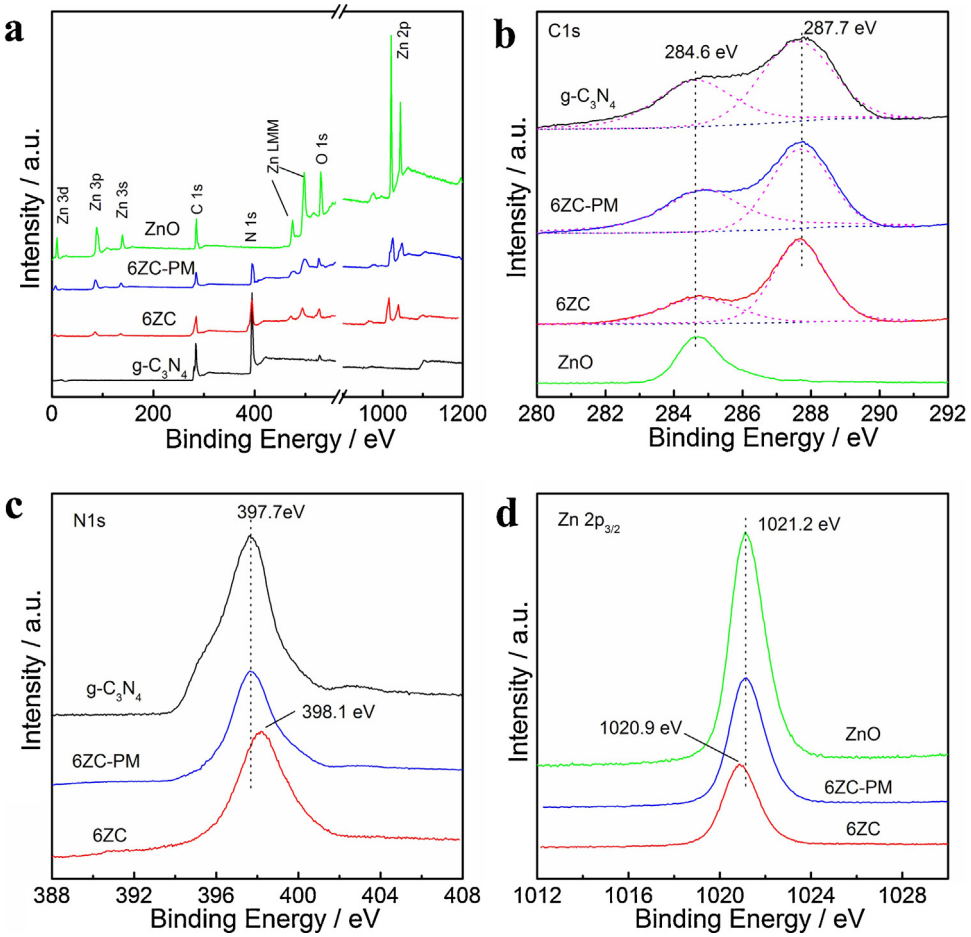

Fig. 3. XPS spectra of ZnO, g-C_3N_4, 6ZC-PM and 6ZC composite. (a) survey spectra, (b) high-resolution spectra of C1s, (c) high-resolution spectra of N1s, (d) high-resolution spectra of Zn2p.

With the exception of the 2ZC sample (which may be due to the low concentration of ZnO), the ZnO/g-C_3N_4 composite gives rise to the characteristic XRD peaks of both ZnO and g-C_3N_4. With increased ZnO content, the XRD peaks of ZnO become stronger. The XRD patterns of 6ZC-PM are also shown in Fig. 1. As expected, both ZnO and g-C_3N_4 are detected. Meanwhile, it can be observed that the ZnO peaks of 6ZC-PM are stronger than those of the 6ZC sample, indicating the 6ZC sample has smaller ZnO particles, which is beneficial for the photocatalytic reaction.

SEM and TEM images were also used to investigate the structure of ZnO/g-C_3N_4 composites. Fig. 2 shows the SEM and TEM images of g-C_3N_4, ZnO and a representative ZnO/g-C_3N_4 sample (6ZC). Pure g-C_3N_4 shows an aggregation of wrinkled sheets (Fig. 2a). Its TEM image further proves that it is highly mesoporous, with pore sizes from 20 ~ 60 nm indicating its high surface area (50.4 m^2/g), which was in line with the literature [28,29] and the BET results (see Fig. S3). ZnO shows triangular and rough spherical particles of about 50 nm on average, with a specific surface area of 34.6 m^2/g. The ZnO/g-C_3N_4 composite displays a morphology similar to pure g-C_3N_4 (Fig. 2e), making it difficult to differentiate ZnO and g-C_3N_4 from the SEM image. However, the ZnO phase can be confirmed thorough EDX results (see Fig. S4). The TEM image further shows the hybrid structure of ZnO/g-C_3N_4, since ZnO is darker than g-C_3N_4. In addition, given that the sample was ultrasonicated during preparation for TEM analysis, the result in Fig. 2f also shows that ZnO nanoparticles are closely coupled with g-C_3N_4. The BET surface area of the ZnO/g-C_3N_4 composite is between those of g-C_3N_4 and ZnO. The BET surface areas of the 2ZC, 4ZC, 6ZC and 8ZC samples are 50, 48.3, 43.0 and 41.5 m^2/g, respectively. With the increase of ZnO content, the specific surface areas of the samples decrease slightly.

The surface chemical compositions of g-C_3N_4, ZnO, ZnO-g-C_3N_4 physical mixture, and the ZnO/g-C_3N_4 composite were analyzed by XPS, with the results shown in Fig. 3. The survey XPS spectra (Fig. 3a) indicate that the prepared ZnO/g-C_3N_4 samples are composed of ZnO and g-C_3N_4, as shown by the strong peaks of C1s, N1s, Zn2p, and O1s. Fig. 3b shows the high-resolution XPS spectra of C1s. For ZnO, only one peak is observed at 284.6 eV, which may be attributed to the adventitious carbon. In the case of g-C_3N_4, 6ZC and 6ZC-PM, another strong C1s peak observed at 287.7 eV can be ascribed to the sp^2-bonded carbon (N—C=N) [30], indicating the existence of g-C_3N_4. The N1s peaks of g-C_3N_4 and 6ZC-PM are located at 397.7 eV. For the 6ZC sample, the N1s peak shifts to 398.1 eV (Fig. 3c). Since all of these originated from C=N—C coordination [30], the change in N1s binding energy indicates the interaction between g-C_3N_4 and ZnO, as reported previously in the literature [31,32]. Similar phenomena are also observed in the Zn 2p XPS spectra. As shown in Fig. 3d, the Zn $2p_{3/2}$ binding energy of 6ZC (1020.9 eV) is slightly lower than those of pure ZnO (1021.2 eV, Zn^{2+}) and 6ZC-PM [33]. Rather than a simple physical mixture, the XPS analyses distinctly suggest the presence of chemical bonds between g-C_3N_4 and ZnO in the ZnO/g-C_3N_4 composite. This kind of interaction is beneficial for the formation of g-C_3N_4/ZnO hetero-junctions and for smooth charge transfer between the two semiconductors. The position of the valence band (VB) edges of g-C_3N_4 and ZnO were also estimated via VB XPS (Fig. S5). The values of g-C_3N_4 and ZnO are determined

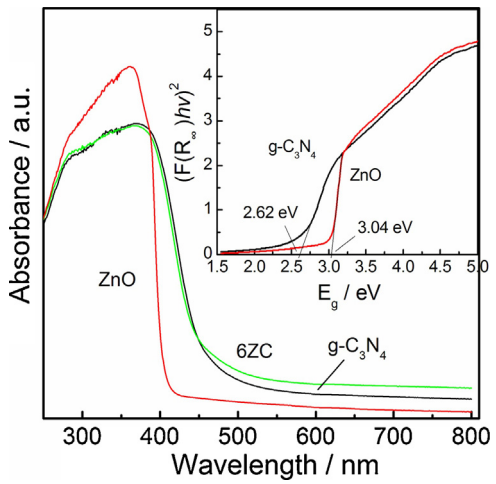

Fig. 4. UV–vis spectra of ZnO, g-C_3N_4, and 6ZC composite. The inset is the plot used to estimate the band gap value by Kubelka–Munk equation.

to be 1.60 and 2.51 eV, respectively, consistent with the results of Kushwaha and Aslam [22] and Fox and Dulay [34].

Fig. 4 shows the UV–vis spectra of ZnO, g-C_3N_4 and the ZnO/g-C_3N_4 composite. Pure g-C_3N_4 has photoabsorption from UV light to visible light, with an absorption edge of 471 nm, originating from a band gap of 2.63 eV. In the case of ZnO, only UV light can be absorbed. The band gap is determined to be 3.04 eV, which is consistent with previous reports [35]. The addition of ZnO shows little effect on the optical property of g-C_3N_4. As shown in Fig. 4, the UV–vis spectrum of 6ZC is nearly the same as pure g-C_3N_4, perhaps due to the low concentration of ZnO and its poor optical properties. Nevertheless, the result in Fig. 4 suggests that ZnO/g-C_3N_4 photocatalysts can absorb visible light.

3.2. Photocatalytic performance of ZnO/g-C_3N_4 composite

The photocatalytic performance of the ZnO/g-C_3N_4 composite was investigated by photocatalytic CO_2 reduction under simulated sunlight irradiation. The blank experiments show that no appreciable amount of product can be detected in the absence of either the photocatalyst or light irradiation, indicating that both the photocatalyst and light irradiation are necessary for photocatalytic CO_2 reduction. After application of the photocatalyst, it was discovered that the main products are CO, methanol, methane and ethanol. CO is the dominant product, a finding consistent with previous work on photocatalytic CO_2 reduction in gas phase [36,37]. (In actuality, from a theoretical standpoint there should be two other products, viz. H_2 and O_2 [38]. However, due to the low sensitivity of the TCD detector and low concentrations of the two products, neither was detected.) A change in the photocatalyst does not greatly affect the distribution of products, but instead affects photocatalytic CO_2 conversion efficiency. As shown in Fig. 5, pure g-C_3N_4 shows a CO_2 reduction rate of 9.4 $\mu mol\, h^{-1}\, g_{cat}{}^{-1}$, which is similar to ZnO, and higher than P25. When ZnO is deposited on g-C_3N_4, the hybrid structure exhibits much higher photocatalytic activity than pure g-C_3N_4. With an increase in ZnO concentration, the photocatalytic activity of ZnO/g-C_3N_4 first increases and then decreases. Sample 6ZC exhibits the highest CO_2 reduction rate of 45.6 $\mu mol\, h^{-1}\, g_{cat}{}^{-1}$, which is 4.9 and 8.2 times higher than those of g-C_3N_4 and P25, respectively. This result clearly indicates that the interaction between ZnO and g-C_3N_4 promotes the formation of hetero-junction structures and generates a novel and highly efficiency photocatalyst.

To further prove the effect and importance of interaction between the components of the ZnO/g-C_3N_4 composite, the

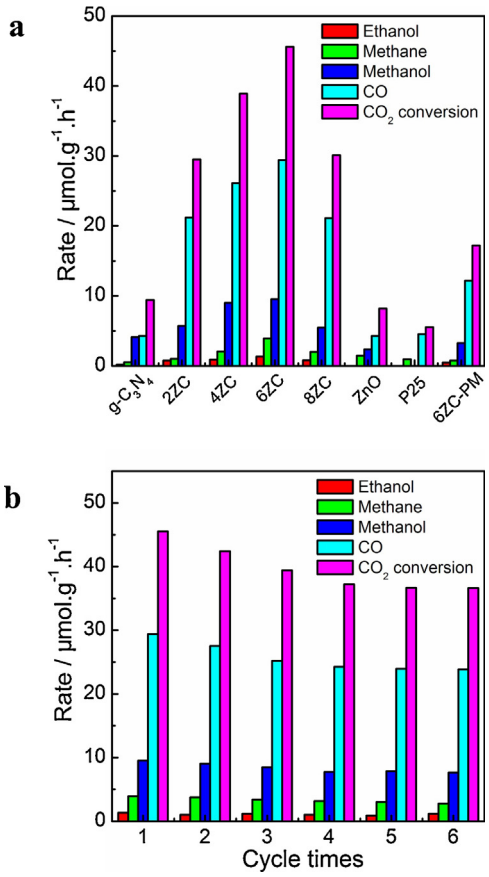

Fig. 5. Photocatalytic activities of g-C_3N_4, ZnO, P25, and ZnO/g-C_3N_4 composites (a) and the cycling run of 6ZC (b).

physical mixture of g-C_3N_4 and ZnO (6ZC-PM) was also prepared and tested through CO_2 photoreduction. The result in Fig. 5a shows that sample 6ZC exhibits much higher photoactivity than 6ZC-PM, even though both have the same phase composition. Clearly, the poor interaction between ZnO and g-C_3N_4 in the 6ZC-PM sample makes the charge transfer between the two components difficult, as a result suppressing their synergetic effect and leading to the mixture's poor photocatalytic activity. Fig. 5b shows the stability of the optimal ZnO/g-C_3N_4 composite (6ZC) by a six-run cycling test of photocatalytic CO_2 reduction. For each run, the sample was dried and then irradiated by a Xe lamp for 4 h. A slight decrease in the CO_2 reduction rate can be observed over the first three cycling runs, after which the rate changes little. This phenomenon is similar to the behavior of some catalysts in their catalytic reaction. For these samples, the decrease in activity was typically attributed to either the inactivation of some active sites or the structural change of the catalyst in the reaction atmosphere [39–41]. Hence, it is possible that some changes might occur in the synthesized ZnO/g-C_3N_4, and XRD and XPS experiments were carried out to detect these. However, no change was observed in the XRD patterns (Fig. S6) and XPS peaks of the used 6ZC sample (Fig. S7). We are still working hard to resolve this issue, but cannot explain it at present. Fortunately, it does not influence our finding that the synthesized ZnO/g-C_3N_4 composite can be seen as a stable photocatalyst.

In addition to the catalyst's stability, the effects of reaction time, CO_2 concentration and reaction temperature on the photocatalytic performance of the ZnO/g-C_3N_4 composite were also investigated; the results are shown in Fig. 6. Under simulated sunlight irradiation for one hour, the generation rates of CO, methanol, methane and ethanol reach 38.7, 19.0, 5.4, 2.5 $\mu mol \cdot g_{cat}{}^{-1}$, respectively, in the presence of the 6ZC photocatalyst (Fig. 6a). With an increase of

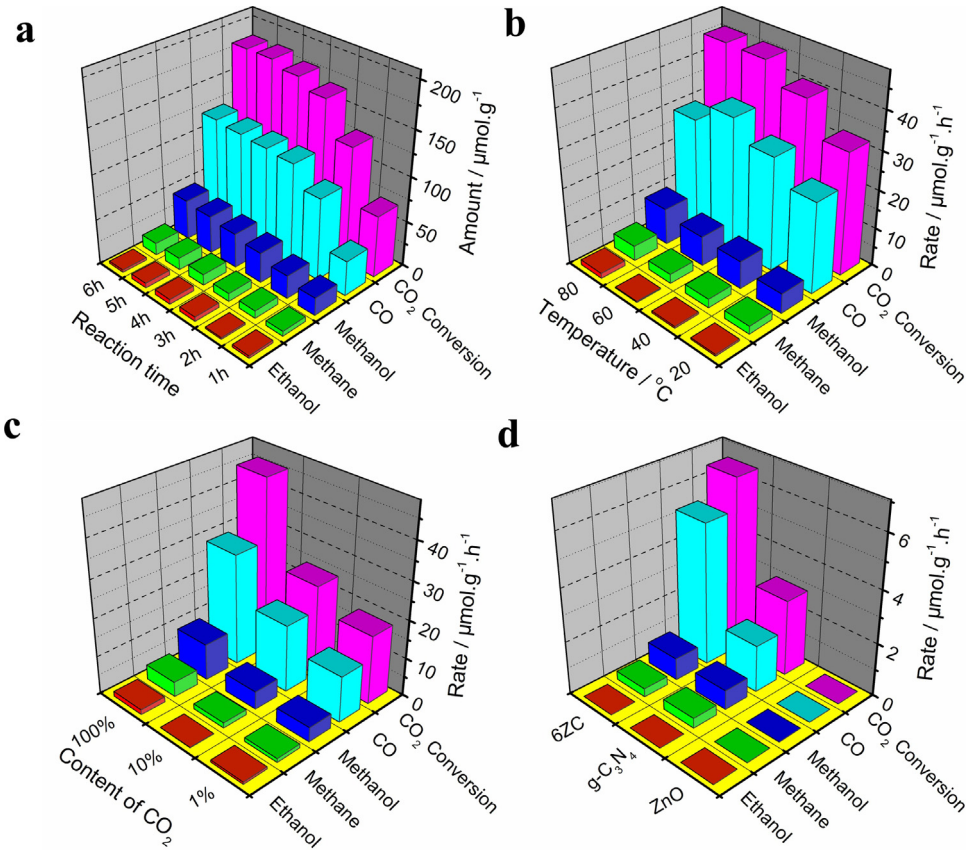

Fig. 6. Effect of reaction time (a), CO_2 content (b), reaction temperature (c) on the photocatalytic performance of 6ZC sample, and the photocatalytic performance of g-C_3N_4, ZnO, and 6ZC under visible light irradiation (d).

reaction time, the generation rate of CO increases rapidly, while the rates of the other products rise more slowly. This might be because CO is more easily generated than the other products, based on their reduction potentials ($CO/CO_2 = -0.11$ V, $CH_4/CO_2 = -0.24$ V, $CH_3OH/CO_2 = -0.32$ V) [42] (the corresponding equations are displayed in the supplementary materials). Because the reaction has achieved balance, the concentration of CO_2 reduction products doesn't increase further after light irradiation exceeds 4 h. Photocatalytic CO_2 reduction resumes only when the generated products are removed (see Fig. 5b).

Fig. 6b shows the effects of reaction temperature on the photocatalytic performance of the ZnO/g-C_3N_4 composite. The reaction temperature usually showed minimal effect on photocatalytic reaction compared to thermal catalytic reaction [43]. Herein, the concentration of H_2O in the gas phase is believed to play an important role. The enhanced temperature can promote the evaporation of water and increase the content of water vapor in the reaction system, which benefits CO_2 reduction, since H_2O is one of the reactants. Therefore, the CO_2 reduction rate increases with the rise of reaction temperature (Fig. 6b). However, after 60 °C, any further increase in temperature contributes little to photocatalytic reaction, as H_2O concentrations are already high enough.

The influence of CO_2 concentration on photocatalytic CO_2 reduction was investigated as well. As shown in Fig. 6c, a decrease in CO_2 content suppresses the photoreduction of CO_2. Nevertheless, even when CO_2 concentration is as low as 1% (diluted by nitrogen), the CO_2 reduction rate still reaches 18.0 μmol h^{-1} $g_{cat}{}^{-1}$, indicating the high efficiency of the ZnO/g-C_3N_4 composite. Fig. 6d shows the photocatalytic performance of g-C_3N_4, ZnO, and the ZnO/g-C_3N_4 composite under visible light irradiation ($\lambda > 420$ nm). Due to its wide band gap, no reduction products are observed in the presence of ZnO. For the g-C_3N_4 and 6ZC samples, the CO_2 conversion rates are 2.88 and 6.54 μmol h^{-1} $g_{cat}{}^{-1}$, respectively. These values are much lower than those under UV–vis light, which may be due to decreased light intensity. In any event, the coupling of ZnO still greatly enhances the photocatalytic activity of g-C_3N_4 under visible light.

3.3. Discussion

The photocatalytic tests demonstrated that the synthesized ZnO/g-C_3N_4 hybrid is an efficient catalyst for photocatalytic CO_2 reduction into fuels for sustainable energy. Although enhanced specific surface area and optical properties are usually beneficial for the activity of photocatalysts, BET and DRS experiments have ruled out this possibility in the case of ZnO/g-C_3N_4. As suggested in the introduction, the promotion effect of ZnO on g-C_3N_4 has been reported previously [23–25]. Although the photocatalytic reaction is different, the origin of the high photoactivity is supposed to be the same. The enhanced photocatalytic efficiency of ZnO/g-C_3N_4 may be ascribed primarily to the efficient separation of electron–hole pairs. As shown in Fig. 7, the conduction band (CB) and valence band (VB) of g-C_3N_4 are determined to be −1.02 and 1.60 eV, respectively, while the band gap positions of ZnO are −0.53 and 2.51 eV. Under irradiation by simulated sunlight, electrons are excited from VB to CB in both g-C_3N_4 and ZnO, generating holes in the VBs of both semiconductors. The photogenerated electrons in g-C_3N_4 can easily migrate to the ZnO surface, while at the same time, the holes in the VB of g-C_3N_4 can transfer to the VB of ZnO. This process can effectively improve photogenerated electron–hole pair separation and greatly decrease the possibility of photogenerated charge recombination, resulting in the high photoactivity of ZnO/g-C_3N_4 composites. This mechanism also explains the different promotion effects of ZnO under simulated sunlight and visible light. For

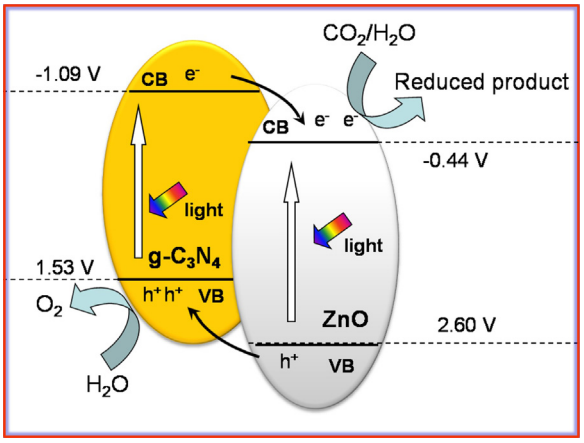

Fig. 7. Schematic illustration of the photocatalytic process for CO_2 reduction on the ZnO/g-C_3N_4 composite.

photocatalytic CO_2 reduction under visible light, only g-C_3N_4 can generate electron–hole pairs. The limited amount of electrons and holes suppresses the photocatalytic activity of the catalyst and lowers the promotion effect of ZnO under visible light compared to UV–vis light.

A series of experiments was conducted to understand photogenerated electron–hole pair separation and electron transfer performance between ZnO and g-C_3N_4. As the PL technique has been generally applied to investigate the separation efficiency of electron–hole pairs in a photocatalyst [44,45], we characterized the PL spectra of the ZnO/g-C_3N_4 composite and g-C_3N_4, respectively. The result in Fig. 8 indicates that ZnO shows weak emission peaks in the range of 400–550 nm, which can be attributed to excitonic PL and results from surface oxygen vacancies and defects of ZnO nanoparticles [45]. Different from ZnO, a strong emission peak centered at about 500 nm was observed in pure g-C_3N_4, which is consistent with the previous report [46]. In the PL spectrum of 6ZC, a weaker emission peak in the same position was detected, suggesting that the addition of ZnO significantly inhibits the recombination of electron–hole pairs [44–46]. For purposes of comparison, the PL spectrum of the physical mixture of ZnO and g-C_3N_4 was also investigated and is displayed in Fig. 8. The result shows that the PL peak of 6ZC-PM is weaker than that of pure g-C_3N_4, but stronger than 6ZC. Although a decreased concentration of g-C_3N_4 would result in a weakened PL peak, the charge transfer between g-C_3N_4 and ZnO would further suppress the recombination of electron–hole pairs, which agrees strongly with the aforementioned mechanism.

The charge transfer between ZnO and g-C_3N_4 semiconductors was also verified by EIS and PC experiments. As shown in Fig. 9a, the

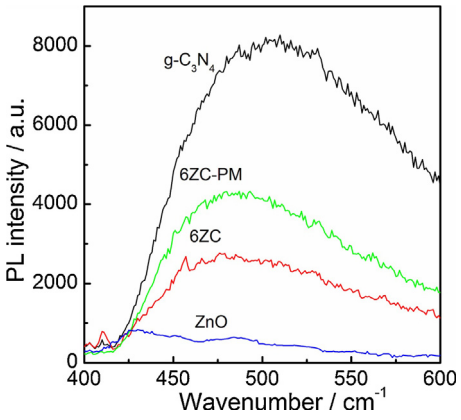

Fig. 8. PL spectra of ZnO, 6ZC, 6ZC-PM, and pure g-C_3N_4 excited at 365 nm.

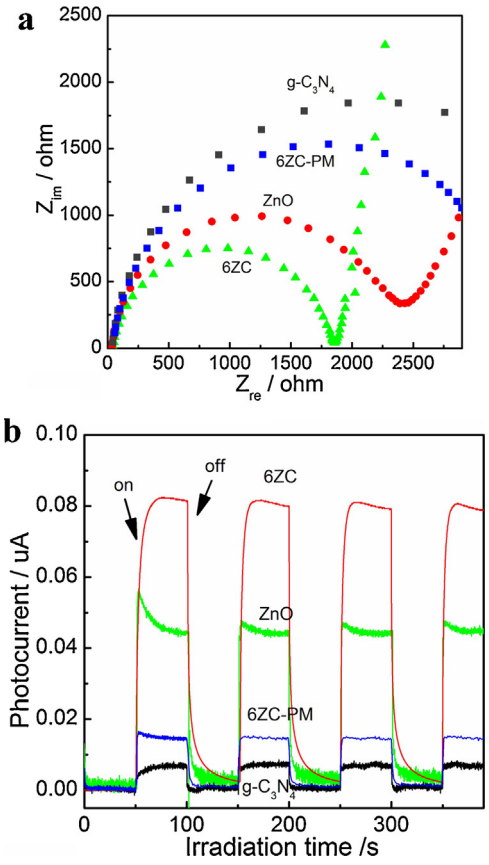

Fig. 9. EIS changes (a) and transient photocurrent responses (b) of g-C_3N_4, ZnO, 6ZC-PM and 6ZC electrodes.

electrode of 6ZC exhibits the smallest arc size. In general, a smaller arc size in an EIS Nyquist plot means smaller charge–transfer resistance on the electrode surface [47,48]. The result in Fig. 9a indicates that the charge separation and electron transfer within the ZnO/g-C_3N_4 electrode is more efficient than in other electrodes. Fig. 9b shows the transient photocurrent responses of the g-C_3N_4, ZnO, 6ZC-PM and 6ZC samples. The photocurrent of 6ZC-PM falls between those of g-C_3N_4 and ZnO, indicating that no synergetic effect exists between the two semiconductors. Fig. 9b also shows a much higher photoelectric current than either pure ZnO or g-C_3N_4 for the ZnO/g-C_3N_4 composite, which suggests that the recombination of electrons and holes is greatly inhibited and the separation of photogenerated charges at the interface between g-C_3N_4 and ZnO is largely improved [48–51]. This result is consistent with the EIS and PL experiments, and demonstrates that the high photocatalytic performance of ZnO/g-C_3N_4 originates from its efficient separation of electron–hole pairs. However, it should be noted that the concentration of ZnO plays a critical role in the photocatalytic activity of the ZnO/g-C_3N_4 composite. Compared with 6ZC, the 8ZC sample shows a lower CO_2 conversion, possibly because excessive deposition of ZnO leads to shielding the active site on g-C_3N_4 surfaces, just as Wang and co-workers proved in their study [52–55]. They found that co-exposure of both consisting semiconductors on the surface is necessary in order to enhance photocatalytic activity in the hetero-junction system [52–55].

4. Conclusion

A simple strategy was developed to synthesize ZnO nanoparticle-functionalized g-C_3N_4 sheets through a simple impregnation method. The synthesized ZnO/g-C_3N_4 exhibits

superior performance for photocatalytic CO_2 reduction due to effective electron–hole pair separation at the composite interfaces, which in turn is based on their band positions and verified by PL and PC experiments, as well as by the band positions of ZnO and g-C_3N_4. This work has the potential to provide new insights into the development of g-C_3N_4-based composites as highly efficient photocatalysts for the conversion of CO_2 to fuel.

Acknowledgements

We acknowledge Dr. Mikel L. Walbridge of the University of Wyoming and Dr. Xiaodong Yi of Xiamen University for their help in XPS analysis. This work was financially supported by the Wyoming Clean Coal Program, the China Scholarship Council, and the Natural Science Foundation of Zhejiang Province in China (LY14B030002).

Appendix A. Supplementary data

Supplementary data associated with this article can be found, in the online version, at http://dx.doi.org/10.1016/j.apcatb.2014.12.017.

References

[1] M. Halmann, Nature 275 (1978) 115–116.
[2] T. Inoue, A. Fujishima, S. Konishi, K. Honda, Nature 277 (1979) 637–638.
[3] Q. Liu, Y. Zhou, J. Kou, X. Chen, Z. Tian, J. Gao, S. Yan, Z. Zou, J. Am. Chem. Soc. 132 (2010) 14385–14387.
[4] S. Navalón, A. Dhakshinamoorthy, M. Álvaro, H. Garcia, ChemSusChem 6 (2013) 562–577.
[5] W.Q. Fan, Q.H. Zhang, Y. Wang, Phys. Chem. Chem. Phys. 15 (2013) 2632–2649.
[6] M. Tahir, N.S. Amin, Renewable Sustainable Energy Rev. 25 (2013) 560–579.
[7] K. Teramura, S. Iguchi, Y. Mizuno, T. Shishido, T. Tanaka, Angew. Chem. 124 (2012) 8132–8135.
[8] K. Teramura, T. Tanaka, H. Ishikawa, Y. Kohno, T. Funabiki, J. Phys. Chem. B 108 (2004) 346–354.
[9] H. Tsuneoka, K. Teramura, T. Shishido, T. Tanaka, J. Phys. Chem. C 114 (2010) 8892–8898.
[10] X.C. Wang, K. Maeda, A. Thomas, K. Takanabe, G. Xin, J.M. Carlsson, K. Domen, M. Antonietti, Nat. Mater. 8 (2009) 76–80.
[11] S.C. Yan, Z.S. Li, Z.G. Zou, Langmuir 25 (2009) 10397–10401.
[12] J. Mao, T.Y. Peng, X.H. Zhang, K. Li, L.Q. Ye, L. Zan, Catal. Sci. Technol. 3 (2013) 1253–1260.
[13] G.C. Xi, S.X. Ouyang, J.H. Ye, Chem. Eur. J. 17 (2011) 9057–9061.
[14] S.C. Yan, S.B. Lv, Z.S. Li, Z.G. Zou, Dalton Trans. 39 (2010) 1488–1491.
[15] Y. Liu, G. Chen, C. Zhou, Y.D. Hu, D.G. Fu, J. Liu, Q. Wang, J. Hazard. Mater. 190 (2011) 75–80.
[16] S.W. Cao, X.F. Liu, Y.P. Yuan, Z.Y. Zhang, Y.S. Liao, J. Fang, S.C.J. Loo, T.C. Sum, C. Xue, Appl. Catal. B: Environ. 147 (2014) 940–946.
[17] Y.P. Yuan, S.W. Cao, Y.S. Liao, L.S. Yin, C. Xue, Appl. Catal. B: Environ. 140–141 (2013) 164–168.
[18] S. Zhou, Y. Liu, J.M. Li, Y.J. Wang, G.Y. Jiang, Z. Zhao, D.X. Wang, A.J. Duan, J. Liu, Y.C. Wei, Appl. Catal.: Environ. 158–159 (2014) 20–29.
[19] Y.P. Zang, L.P. Li, Y. Zuo, H.F. Lin, G.S. Li, X.F. Guan, RSC Adv. 3 (2013) 13646–13650.
[20] Y.X. Ji, J.F. Cao, L.Q. Jiang, Y.H. Zhang, Z.G. Yi, J. Alloys Compd. 590 (2014) 9–14.
[21] S.M. Wang, D.L. Li, C. Sun, S.G. Yang, Y. Guan, H. He, Appl. Catal. B: Environ. 144 (2014) 885–892.
[22] A. Kushwaha, M. Aslam, Electrochim. Acta 130 (2014) 222–231.
[23] Y.J. Wang, R. Shi, J. Lin, Y.F. Zhu, Energy Environ. Sci. 4 (2011) 2922–2929.
[24] W. Liu, M.L. Wang, C.X. Xu, S.F. Chen, X.L. Fu, J. Mol. Catal. A: Chem. 368–369 (2013) 9–15.
[25] J.X. Sun, Y.P. Yuan, L.G. Qiu, X. Jiang, A.J. Xie, Y.H. Shen, J.F. Zhu, Dalton Trans. 41 (2012) 6756–6763.
[26] M.C. Long, W.M. Cai, H. Kisch, J. Phys. Chem. C 112 (2008) 548–554.
[27] T.T. Li, Y.M. He, H.J. Lin, J. Cai, L.Z. Dong, X.X. Wang, M.F. Luo, L.H. Zhao, X.D. Yi, W.Z. Weng, Appl. Catal. B: Environ. 138–139 (2013) 95–103.
[28] F. Dong, L.W. Wu, Y.J. Sun, M. Fu, Z.B. Wu, S.C. Lee, J. Mater. Chem. 21 (2011) 15171–15174.
[29] Y.W. Zhang, J.H. Liu, G. Wu, W. Chen, Nanoscale 4 (2012) 5300–5303.
[30] H. Xu, J. Yan, Y.G. Xu, Y.H. Song, H.M. Li, J.X. Xia, C.J. Huang, H.L. Wan, Appl. Catal. B: Environ. 129 (2013) 182–193.
[31] C.S. Pan, J. Xu, Y.J. Wang, D. Li, Y.F. Zhu, Adv. Funct. Mater. 22 (2012) 1518–1524.
[32] X.X. Wang, S.S. Wang, W.D. Hu, J. Cai, L.H. Zhang, L.Z. Dong, L.H. Zhao, Y.M. He, Mater. Lett. 115 (2014) 53–56.
[33] X.J. Wang, W. Wang, Y.L. Liu, Sens. Actuators B 168 (2012) 39–45.
[34] M.A. Fox, M.T. Dulay, Chem. Rev. 93 (1993) 341–357.
[35] V. Srikant, D.R. Clarke, J. Appl. Phys. 83 (1998) 5447–5451.
[36] K.K. Adachi Ohta, T. Mizuno, Sol. Energy Mater. Sol. Cells 53 (1994) 187–190.
[37] Y. Li, W.N. Wang, Z.L. Zhan, M.H. Woo, C.Y. Wu, P. Biswas, Appl. Catal. B Environ. 100 (2010) 386–392.
[38] V. Jeyalakshmi, K. Rajalakshmi, R. Mahalakshmy, K.R. Krishnamurthy, B. Viswanathan, Res. Chem. Intermed. 39 (2013) 2565–2602.
[39] Y.D. Hou, X.C. Wang, L. Wu, Z.X. Ding, X.Z. Fu, Environ. Sci. Technol. 40 (2006) 5799–5803.
[40] X.L. Fu, X.X. Wang, Z.X. Ding, D.Y.C. Leung, Z.Z. Zhang, J.L. Long, W.X. Zhang, Z.H. Li, X.Z. Fu, Appl. Catal. B: Environ. 91 (2009) 67–72.
[41] P. Konova, A. Naydenov, C.V. Venkov, D. Mehandjiev, D. Andreeva, T. Tabakova, J. Mol. Catal. A: Chem. 213 (2004) 235–240.
[42] G.H. Liu, N. Hoivik, K.Y. Wang, H. Jakobsen, Sol. Energy Mater. Sol. Cells 105 (2012) 53–68.
[43] X.Z. Fu, W.A. Zeltner, M.A. Anderson, Appl. Catal. B: Environ. 6 (1995) 209–224.
[44] Y.M. He, L.H. Zhang, X.X. Wang, Y. Wu, H.J. Lin, L.H. Zhao, W.Z. Weng, H.L. Wan, M. Fan, RSC Adv. 4 (2014) 13610–13619.
[45] L.Q. Jing, Y.C. Qu, B.Q. Wang, S.D. Li, B.J. Jiang, L.B. Yang, W. Fu, H.G. Fu, J.Z. Sun, Sol. Energy Mater. Sol. Cells 90 (2006) 1773–1787.
[46] K. Sridharan, E. Jang, T.J. Park, Appl. Catal. B: Environ. 143 (2013) 718–728.
[47] Y.M. He, J. Cai, L.H. Zhang, X.X. Wang, H.J. Lin, B.T. Teng, L.H. Zhao, W.Z. Weng, H.L. Wan, M. Fan, Ind. Eng. Chem. Res. 53 (2014) 5905–5915.
[48] H.T. Yu, X. Quan, S. Chen, H.M. Zhao, Y.B. Zhang, J. Photochem. Photobiol. A: Chem. 200 (2008) 301–306.
[49] J. Lim, D. Monllor-Satocaa, J.S. Jang, S. Lee, W. Choi, Appl. Catal. B: Environ. 152–153 (2014) 233–240.
[50] L.Z. Dong, Y.M. He, T.T. Li, J. Cai, W.D. Hu, S.S. Wang, H.J. Lin, M.F. Luo, X.D. Yi, L.H. Zhao, W.Z. Weng, H.L. Wan, Appl. Catal. A: Gen. 472 (2014) 143–151.
[51] Y.P. Bi, S.X. Ouyang, J.Y. Cao, J.H. Ye, Phys. Chem. Chem. Phys. 13 (2011) 10071–10075.
[52] X. Wang, Q. Xu, M.R. Li, S. Shen, X.L. Wang, Y.C. Wang, Z.C. Feng, J.Y. Shi, H.X. Han, C. Li, Angew. Chem. Int. Ed. 51 (2012) 13089–13092.
[53] Y.S. Jia, S. Shen, D.G. Wang, X. Wang, J.Y. Shi, F.X. Zhang, H.X. Han, C. Li, J. Mater. Chem. A 1 (2013) 7905–7912.
[54] X. Wang, S. Shen, S.Q. Jin, J.X. Yang, M.R. Li, X.L. Wang, H.X. Han, C. Li, Phys. Chem. Chem. Phys. 15 (2013) 19380–19386.
[55] J. Zhang, Q. Xu, Z. Feng, M. Li, C. Li, Angew. Chem. Int. Ed. 47 (2008) 1766–1769.